Rare Met. (2019) 38(1):29–34
https://doi.org/10.1007/s12598-014-0434-9

RARE METALS
www.editorialmanager.com/rmet

Hydrothermal synthesis mechanism and electrochemical performance of $LiMn_{0.6}Fe_{0.4}PO_4$ cathode material

Chang-Chang Xu, Ying Wang, Li Li, Yi-Jing Wang*, Li-Fang Jiao, Hua-Tang Yuan

Received: 23 December 2013 / Revised: 11 March 2014 / Accepted: 15 December 2014 / Published online: 4 January 2015

Abstract Monocrystal $LiMn_{0.6}Fe_{0.4}PO_4$ cathode material was obtained via hydrothermal method at 180 °C for 10 h without any surfactant. The effects of hydrothermal time on the phase and morphology of the material were discussed. By controlling the reaction solutions, the rodlike, flowerlike, and strawlike $LiMn_{0.6}Fe_{0.4}PO_4$ cathode materials were synthesized. Electrochemical performances show that the rodlike $LiMn_{0.6}Fe_{0.4}PO_4$ has the best electrochemical properties. The initial discharge capacity of the rodlike structure is 106.4 $mAh \cdot g^{-1}$, which is higher than those of flowerlike and strawlike materials.

Keywords $LiMn_{0.6}Fe_{0.4}PO_4$; Hydrothermal method; Cathode material; Lithium-ion batteries; Synthesis mechanism

C.-C. Xu, Y. Wang, L. Li, Y.-J. Wang*, L.-F. Jiao, H.-T. Yuan
Institute of New Energy Material Chemistry, Nankai University, Tianjin 300071, China
e-mail: wangyj@nankai.edu.cn

C.-C. Xu, Y. Wang, L. Li, Y.-J. Wang, L.-F. Jiao, H.-T. Yuan
Collaborative Innovation Center of Chemical Science and Engineering (Tianjin), Nankai University, Tianjin 300071, China

C.-C. Xu, Y. Wang, L. Li, Y.-J. Wang, L.-F. Jiao, H.-T. Yuan
Key Laboratory of Advanced Energy Materials Chemistry, Nankai University, Tianjin 300071, China

C.-C. Xu, Y. Wang, L. Li, Y.-J. Wang, L.-F. Jiao, H.-T. Yuan
Tianjin Key Laboratory on Metal and Molecule-based Material Chemistry, Nankai University, Tianjin 300071, China

1 Introduction

Lithium-ion batteries, which have high energy density and efficiency, become more and more popular [1–10]. As a typical cathode, $LiMn_xFe_{1-x}PO_4$ materials have advantages of environmental benignity, low cost, high capacity, excellent cycle life, and thermal stability; all of these make them be promising materials. The redox potential of Mn^{3+}/Mn^{2+} versus Li^+/Li is 4.1 V, higher than that of Fe^{3+}/Fe^{2+}. It indicates that Mn-based olivine structural $LiMn_xFe_{1-x}PO_4$ offers a higher energy density than $LiFePO_4$. Meanwhile, $LiMn_xFe_{1-x}PO_4$ shows much better electrochemical property compared with $LiMnPO_4$. The main reason is that doping Fe^{2+} into olivine structure significantly reduces the volume changes caused by the Jahn–Teller effect around Mn^{3+}. Therefore, great attention was paid to Mn-based olivine-structured $LiMn_xFe_{1-x}PO_4$ materials [11–13].

Recently, $LiMn_xFe_{1-x}PO_4$ materials with various morphologies were successfully synthesized due to the effect of shape on the electrochemical property. Many experiments suggested that $LiMPO_4$ (M = Mn, Fe) materials assembled by different shapes were prepared with various surfactants [14–19], but the discussion about the effects of the morphology of the materials on the electrochemical performances should eliminate the differences of surfactants. So it is essential to overcome challenges in the preparation of monocrystal $LiMn_xFe_{1-x}PO_4$ without any surfactant.

In this work, a facile hydrothermal method to prepare monocrystal $LiMn_{0.6}Fe_{0.4}PO_4$ material without any surfactant was reported. The possible synthesis and formation mechanism of strawlike $LiMn_{0.6}Fe_{0.4}PO_4$ were proposed on the basis of time-dependent experiments. Moreover, the influential factor such as solvent was also investigated.

Rodlike, flowerlike, and strawlike $LiMn_{0.6}Fe_{0.4}PO_4$ materials were synthesized, and their differences on the electrochemical performances were studied.

2 Experimental

2.1 Synthesis of $LiMn_{0.6}Fe_{0.4}PO_4$ materials

$LiMn_{0.6}Fe_{0.4}PO_4$ cathode materials were synthesized by a facile hydrothermal method. $Li_2SO_4{\cdot}H_2O$, $NH_4H_2PO_4$, $MnSO_4{\cdot}H_2O$, and $(NH_4)_2Fe(SO_4)_2{\cdot}6H_2O$ with mole ratio of 2.0:1.0:0.6:0.4 were dissolved into 27 ml distilled water with magnetic stirring, resulting in a transparent liquid. And then 1 ml hydrazine hydrate was dropped into the solution. At last, the mixture was transferred into 40-ml Teflon-lined autoclave, which was maintained at 180 °C for 10 h and cooled down to room temperature naturally. The product was filtered, washed, and dried under vacuum at 80 °C for 10 h. After annealing in argon–hydrogen atmosphere at 300 °C for 5 h, the sample was achieved.

2.2 Characterization

The crystalline forms of the synthesized materials were characterized by X-ray power diffraction (XRD, Rigaku D/Max-2500, Cu Kα radiation) with scanning rate of 1.2 (°)·min^{-1} and 2θ range of 3°–80°. Scanning electron microscopy (SEM, Hitachi X-650) equipped with energy dispersive spectrometer (EDS), transmission electron microscopy (TEM, JEOL JEM-2100), and X-ray photoelectron spectrometer (XPS, PHI 5000 Versaprobe, ULVACPHI) were used to analyze the surface morphology, element compositions, and valence states of the sample.

2.3 Electrochemical property

The as-prepared sample was mixed with 20 % acetylene black and heated at 600 °C for 10 h in Ar/5 % H_2 gas flow. Then, they were combined with polyvinylidene fluoride (PVDF) in weight ratio of 90:10, pasted on an aluminum foil and finally dried in vacuum oven at 100 °C for 10 h. Electrolyte cells were assembled with the cathodes as-fabricated, lithium foil Celgard 2300 film separator and 1 mol·L^{-1} $LiFP_6$ that was dissolved into a mixture of ethylene carbonate (EC) and dimethyl carbonate (DMC) (1:1; volume ratio). After that, the cells were charged with C/20 rate to 4.5 V, kept at 4.5 V until C/80 rate, and then discharged to 2.3 V at C/20 rate on a LAND battery-test instrument (CT2001A). All the tests were carried out at room temperature.

3 Results and discussion

3.1 Materials characterization

Figure 1 displays the XRD patterns of the synthesized $LiMn_{0.6}Fe_{0.4}PO_4$. All the diffraction peaks of $LiMn_{0.6}Fe_{0.4}PO_4$ materials can be identified to $LiMn_{0.6}Fe_{0.4}PO_4$ phase with an orthorhombic olivine structure, and its space group is *Pnma* according to the standard card (JCPDS 74-375). The lattice parameters can be obtained by calculating from the XRD pattern of $LiMn_{0.6}Fe_{0.4}PO_4$ composite on general structure analysis system (GSAS). The lattice parameters are $a = 0.6058$ nm, $b = 1.0423$ nm, and $c = 0.4736$ nm, which are close to the previous results [20]. The valence states of Mn and Fe are illustrated in Fig. 2. As shown in Fig. 2a, a single peak with binding energy of 641.8 eV demonstrates that the valence state of Mn is +2. Correspondingly, a wide peak of binding energy at 711.4 eV declares that the oxidation state of Fe is +2, in agreement with the report of Zhang et al. [18]. Moreover, the EDS spectrum of the material is shown in Fig. 2c. It reveals that Mn, Fe, P, and O elements are all observed in $LiMn_{0.6}Fe_{0.4}PO_4$ composite except Li due to its light weight. Furthermore, the relative ratio of Mn and Fe is 6:4 from EDS analysis. Therefore, it can be confirmed that pure $LiMn_{0.6}Fe_{0.4}PO_4$ material is successfully synthesized.

SEM and TEM images of $LiMn_{0.6}Fe_{0.4}PO_4$ material are shown in Fig. 3a and b. It is found that strawlike $LiMn_{0.6}Fe_{0.4}PO_4$ assembled by rods is about 10–20 μm in diameter. Moreover, the SAED pattern is shown in Fig. 3c, it is found that there are a series of periodic two-dimensional diffraction points, which demonstrate that the structure of synthesized $LiMn_{0.6}Fe_{0.4}PO_4$ materials is single crystal.

3.2 Hydrothermal synthesis mechanism

A set of experiments with different hydrothermal time (0, 2, 4, 6 h) were carried out in order to discuss the synthesis

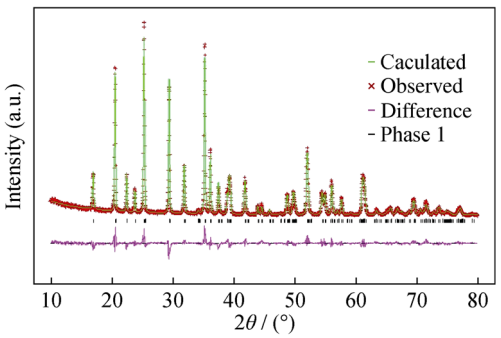

Fig. 1 Rietveld refinement patterns of XRD data for $LiMn_{0.6}Fe_{0.4}PO_4$ powder

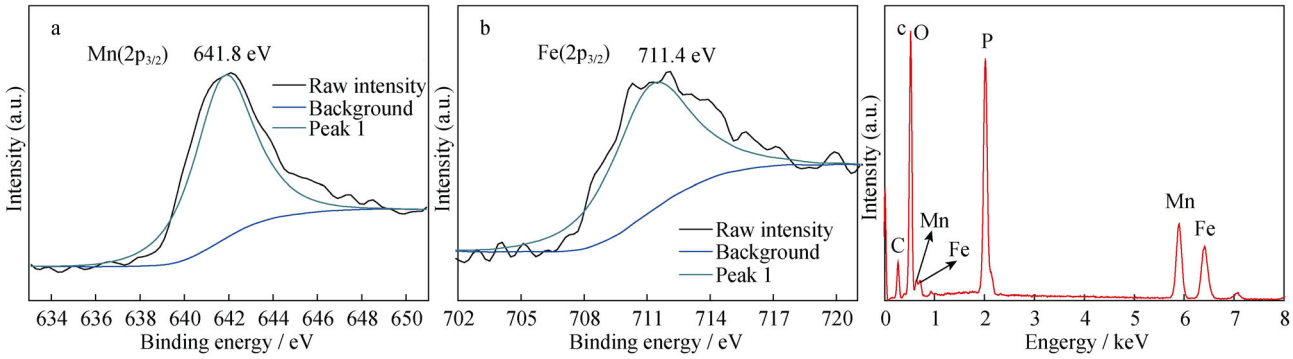

Fig. 2 XPS spectra of **a** Mn $2p_{3/2}$ and **b** Fe $2p_{3/2}$ of $LiMn_{0.6}Fe_{0.4}PO_4$ sample, and **c** EDS result of $LiMn_{0.6}Fe_{0.4}PO_4$ sample

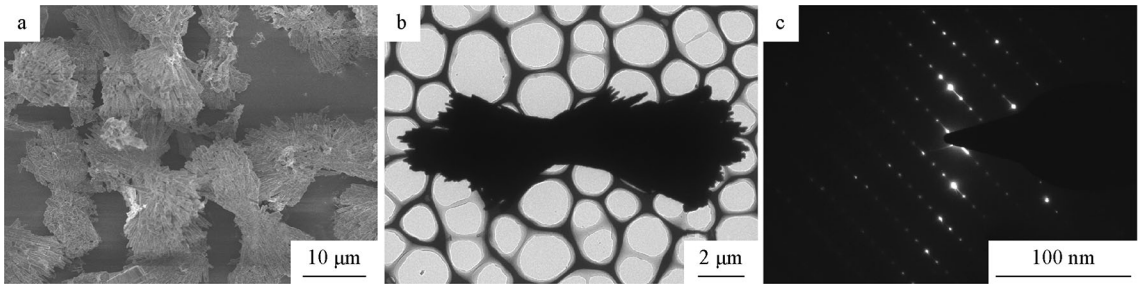

Fig. 3 SEM image **a**, TEM image **b**, and corresponding SAED pattern **c** of $LiMn_{0.6}Fe_{0.4}PO_4$ sample

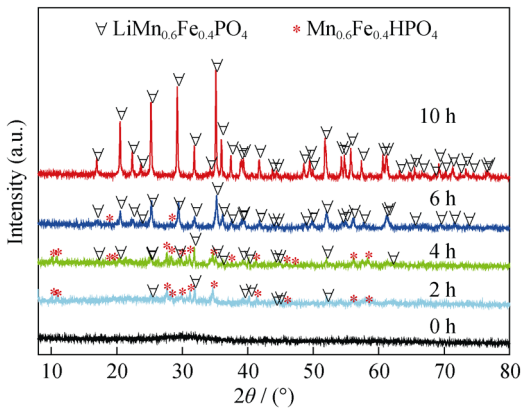

Fig. 4 XRD patterns of samples prepared for different hydrothermal time

mechanism of the $LiMn_{0.6}Fe_{0.4}PO_4$ material. The effect of hydrothermal time on the phase and morphology were characterized by XRD and SEM analysis.

The XRD patterns of the samples prepared for different hydrothermal time are shown in Fig. 4. After the addition of hydrazine hydrate, the pH value of the solution was adjusted to 9–10. There is very little amount of HPO_4^{2-} in the solution. Moreover, according to the solubility product constants (K_{sp}), it is found that the K_{sp} of $MnHPO_4$ and $FeHPO_4$ are very close to each other and they are both smaller than those of $Mn(OH)_2$, $Fe(OH)_2$, NH_4MnPO_4, and NH_4FePO_4. Therefore, based on the fundamental of chemical precipitation, Mn^{2+} and Fe^{2+} could react with HPO_4^{2-} simultaneously. Thus, $Mn_{0.6}Fe_{0.4}HPO_4$ composite is achieved. When hydrothermal reaction time is 2, 4, or 6 h, the peaks of $Mn_{0.6}Fe_{0.4}HPO_4$ appear and coincide with the standard card (JCPDS 74-199) [16], indicating that amorphous $Mn_{0.6}Fe_{0.4}HPO_4$ gradually transforms into crystal $Mn_{0.6}Fe_{0.4}HPO_4$. Moreover, the diffraction peaks of $LiMn_{0.6}Fe_{0.4}PO_4$ matched with JCPDS 74-375 are also observed. With the increase of the hydrothermal time, the amounts of diffraction peaks of $LiMn_{0.6}Fe_{0.4}PO_4$ increase gradually, while those of $Mn_{0.6}Fe_{0.4}HPO_4$ disappear little by little.

Based on these analyses, the possible hydrothermal synthesis mechanism of $LiMn_{0.6}Fe_{0.4}PO_4$ material is proposed as follows: at the early reaction stage, hydrazine hydrate is hydrolyzed to yield hydroxyl, and then the hydroxyl reacts with H_2PO_4. Thus, HPO_4^{2-} is obtained as shown in Reactions (1) and (2). Amorphous $Mn_{0.6}Fe_{0.4}HPO_4$ firstly forms through Reaction (3). As the hydrothermal reaction goes on, $LiMn_{0.6}Fe_{0.4}PO_4$ finally generates after the $Mn_{0.6}Fe_{0.4}HPO_4$ reacts with Li^+ through Reaction (4).

$$N_2H_4^+ + H_2O \rightarrow N_2H_5^+ + OH^- \quad (1)$$

$$OH^- + H_2PO_4^- \rightarrow HPO_4^{2-} + H_2O \quad (2)$$

$$0.6\ Mn^{2+} + 0.4\ Fe^{2+} + HPO_4^{2-} \rightarrow Mn_{0.6}Fe_{0.4}HPO_4 \downarrow \quad (3)$$

$$Mn_{0.6}Fe_{0.4}HPO_4 + Li^+ \rightarrow LiMn_{0.6}Fe_{0.4}PO_4 \downarrow + H^+ \quad (4)$$

Meanwhile, Fig. 5 shows the possible formation mechanism of strawlike $LiMn_{0.6}Fe_{0.4}PO_4$ materials. Amorphous $Mn_{0.6}Fe_{0.4}HPO_4$ is composed of nano-particles before the hydrothermal reaction. As the hydrothermal reaction goes on, the $Mn_{0.6}Fe_{0.4}HPO_4$ nano-particles disappear, while self-assembly structures appear gradually. Strawlike $LiMn_{0.6}Fe_{0.4}PO_4$ assembled with rods was prepared at last. The possible formation mechanism is also illustrated in Fig. 6.

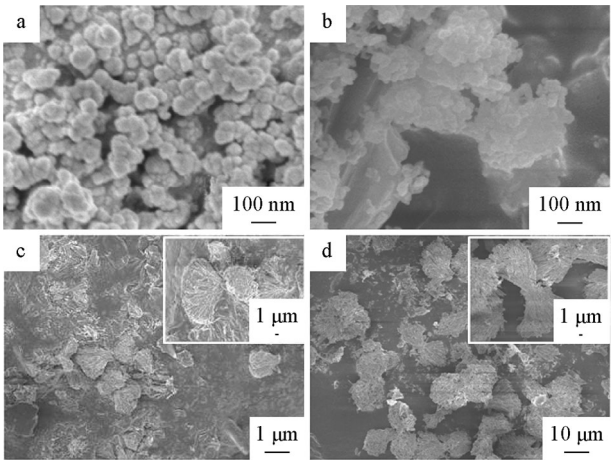

Fig. 5 SEM images of samples prepared for different hydrothermal time: **a** 0 h, **b** 2 h, **c** 6 h, and **d** 10 h. Inserts in **c** and **d** being corresponding enlarged images

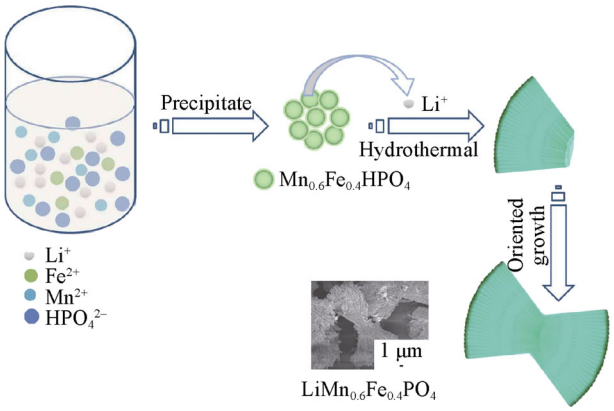

Fig. 6 Schematic illustration of hydrothermal synthesis mechanism of $LiMn_{0.6}Fe_{0.4}PO_4$ material

3.3 Effect of solvent

In order to investigate the effect of the reaction solvent on the morphology of the samples, a series of experiments were carried out. The distilled water was replaced by water–ethanediol (2:1; volume ratio) or water–isopropanol (2:1; volume ratio), while the other factors were kept the same. Using water–ethanediol (2:1; volume ratio) as the reactive solvent, flowerlike $LiMn_{0.6}Fe_{0.4}PO_4$ materials can be achieved (Fig. 7b). The particle size of the flowerlike $LiMn_{0.6}Fe_{0.4}PO_4$ material is about 5 μm. Figure 7c illustrates that rodlike $LiMn_{0.6}Fe_{0.4}PO_4$ can form by employing the mixture solution of water–isopropanol (2:1; volume ratio). It is found that the width of the rods is about 300 nm and the length is around 1 μm. Obviously, $LiMn_{0.6}Fe_{0.4}PO_4$ materials with various shapes were prepared with different solvents such as water, water–ethylene glycol, or isopropanol were utilized. It may be related to the polarities of solvents [21]. The polarities of solvents may have an effect on the growth of $LiMn_{0.6}Fe_{0.4}PO_4$ material. The sequence of the polarities of solvents is water, ethylene glycol, and isopropanol from large to small order. Combining the polarities of solvents with the SEM results of $LiMn_{0.6}Fe_{0.4}PO_4$ materials prepared under different solvents, it declares that $LiMn_{0.6}Fe_{0.4}PO_4$ materials may prefer to self-assemble in the bigger polarity of solvents such as water and ethylene glycol.

Moreover, the electrochemical performances of rodlike, flowerlike, and strawlike $LiMn_{0.6}Fe_{0.4}PO_4$ materials were tested at a 0.05C rate. The first charge/discharge capacity and cycling properties of the above $LiMn_{0.6}Fe_{0.4}PO_4$ materials are illustrated in Fig. 8a and b. It is found that there are two characteristic potential plateaus related to Fe and Mn in Fig. 8a. As to the first plateau near 3.5 V, it is

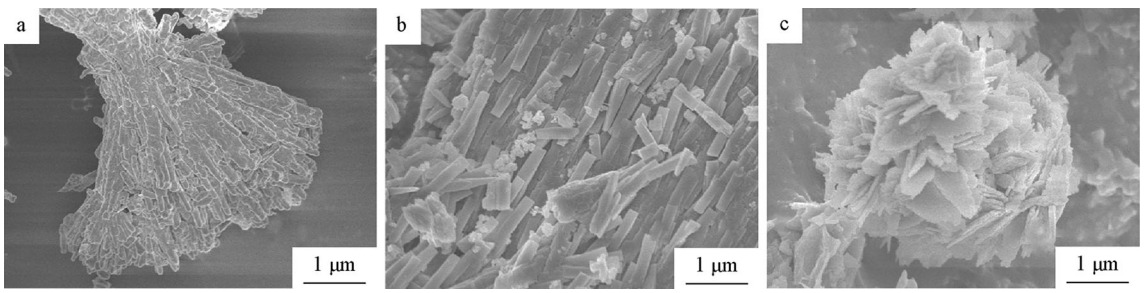

Fig. 7 SEM images of $LiMn_{0.6}Fe_{0.4}PO_4$ samples obtained from different reaction solvents: **a** water, **b** water–ethanediol, and **c** water–isopropanol

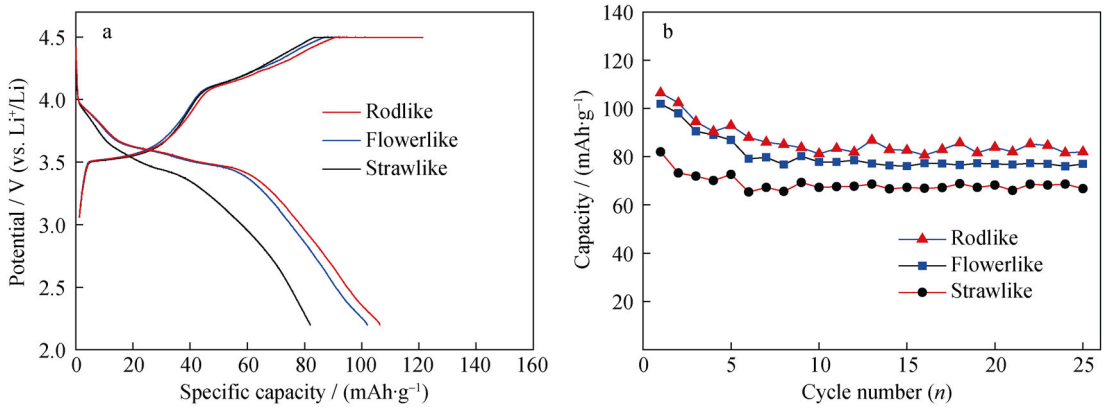

Fig. 8 Charge–discharge curves **a** and cycling performance plots **b** of $LiMn_{0.6}Fe_{0.4}PO_4$ with strawlike, flowerlike, and rodlike at 0.05C rate

associated to the redox process of Fe^{3+}/Fe^{2+}. Similarly, the redox process of Mn^{3+}/Mn^{2+} causes the second plateau at around 4.0 V. Obviously, the capacity related to Mn^{3+}/Mn^{2+} is low, it is preferable to account it to the polarization effect caused by the diffusion rate of lithium ions and the poor electro-conductivity of LMFP material [22]. The initial discharge capacities of rodlike, flowerlike, and strawlike $LiMn_{0.6}Fe_{0.4}PO_4$ materials are only 106.4, 101.9, and 82.0 $mAh \cdot g^{-1}$, respectively. It can be confirmed that rodlike $LiMn_{0.6}Fe_{0.4}PO_4$ material has the best electrochemical property. The reason may be that the size of rodlike material is much smaller than those of others. Furthermore, the ideal crystal of the rods is beneficial to the diffusion of lithium ions [17], which also plays a significant role in enhancing the electrochemical performance.

4 Conclusion

In this study, a facile hydrothermal method for the preparation of monocrystal $LiMn_{0.6}Fe_{0.4}PO_4$ materials was demonstrated. Based on the time-dependent experiments and the fundamental of chemical precipitation, the possible synthesis mechanism was proposed. Rodlike, flowerlike, and strawlike $LiMn_{0.6}Fe_{0.4}PO_4$ materials were synthesized by controlling the composition of the solution. In comparison with flowerlike and strawlike $LiMn_{0.6}Fe_{0.4}PO_4$ materials, rodlike $LiMn_{0.6}Fe_{0.4}PO_4$ materials have the best electrochemical property due to its small particle size and the special shape.

Acknowledgments This work was financially supported by the National Natural Science Foundation of China (Nos. 21231005 and 51071087), the Major State Basic Research Development Program of China (Nos. 2011CB935900 and 2010CB631303), the Discipline Innovative Engineering Plan (B12015), the Research Fund for the Doctoral Program of Higher Education of China (No. 20120031110001), and the Tianjin Science & Technology Project (No. 10SYSYJC27600).

References

[1] Ellis BL, Lee KT, Nazar LF. Positive electrode materials for Li-ion and Li-batteries. Chem Mater. 2010;22(3):691.
[2] Bi J, Shao S, Guan W, Wang L. State of charge estimation of Li-ion batteries in electric vehicle based on radial-basis-function neural network. Chin Phys B. 2012;21(11):118801.
[3] Marom R, Amalraj SF, Leifer N, Jacob D, Aurbach D. A review of advanced and practical lithium battery materials. J Mater Chem. 2011;21(27):9938.
[4] Pitchai R, Thavasi V, Mhaisalkar SG, Ramakrishna S. Nanostructured cathode materials: a key for better performance in Li-ion batteries. J Mater Chem. 2011;21(30):11040.
[5] Li H, Wang ZX, Chen LQ, Huang XJ. Research on advanced materials for Li-ion batteries. Adv Mater. 2009;21(45):4593.
[6] Song HK, Lee KT, Kim MG, Nazar LF, Cho J. Recent progress in nanostructured cathode materials for lithium secondary batteries. Adv Funct Mater. 2010;20(22):3818.
[7] Wu Y, Pei F, Jia LL, Liu XL, Zhang WH, Liu P. Overview of recovery technique of valuable metals from spent lithium ion batteries. Chin J Rare Met. 2013;37(2):320.
[8] Xin XG, Shen JQ, Shi SQ. Structural and magnetic properties of $LiNi_{0.5}Mn_{1.5}O_4$ and $LiNi_{0.5}Mn_{1.5}O_{4-\delta}$ spinels: a first-principles study. Chin Phys B. 2012;21(12):128202.
[9] Yang LJ, Wang JL, Yang CT, Mei LR. Preparation of silicon nanowires by hydrothermal and its physical properties. Chin J Rare Met. 2013;37(4):564.
[10] Ban LQ, Zhuang WD, Lu HQ, Yin YP, Wang Z. Progress in modification of layered cathode material Li-Ni-Co-Mn-O. Chin J Rare Met. 2013;37(5):820.
[11] Kim J, Seo DH, Kim SW, Park YU, Kang K. Mn based olivine electrode material with high power and energy. Chem Commun. 2010;46(8):1305.
[12] Martha SK, Grinblat J, Haik O, Zinigrad E, Drezen T, Miners JH, Exnar I, Kay A, Markovsky B, Aurbach D. $LiMn_{0.8}Fe_{0.2}PO_4$: an advanced cathode material for rechargeable lithium batteries. Angew Chem Int Ed. 2009;48(45):8559.
[13] Wang H, Yang Y, Liang Y, Cui LF, Casalongue HS, Li Y, Hong G, Cui Y, Dai H. $LiMn_{1-x}Fe_xPO_4$ nanorods grown on graphene sheets for ultrahigh-rate-performance lithium ion batteries. Angew Chem Int Ed. 2011;50(32):7364.
[14] Guo YQ, Huang R, Song J, Wang X, Song C, Zhang YX. Growth characteristics of amorphous-layer-free nanocrystalline silicon films fabricated by very high frequency PECVD at 250 C. Chin Phys B. 2012;21(6):066106.

[15] Wang YR, Yang YF, Yang YB, Shao HX. Fabrication of microspherical $LiMnPO_4$ cathode material by a facile one-step solvothermal process. Mater Res Bull. 2009;44(11):2139.
[16] Pan XL, Xu CY, Zhen L. Synthesis of $LiMnPO_4$ microspheres assembled by plates, wedges and prisms with different crystallographic orientations and their electrochemical performance. CrystEngComm. 2012;14(20):6412.
[17] Nie P, Shen LF, Zhang F, Chen L, Deng HF, Zhang XG. Flower-like $LiMnPO_4$ hierarchical microstructures assembled from single-crystalline nanosheets for lithium-ion batteries. CrystEngComm. 2012;14(13):4284.
[18] Zhang Y, Sun CS, Zhou Z. Sol-gel preparation and electrochemical performances of $LiFe_{1/3}Mn_{1/3}Co_{1/3}PO_4$/C composites with core-shell nanostructure. Electrochem Commun. 2009; 11(6):1183.
[19] Wang F, Yang J, Gao PF, NuLi YN, Wang JL. Morphology regulation and carbon coating of $LiMnPO_4$ cathode material for enhanced electrochemical performance. J Power Sources. 2011;196(23):10258.
[20] Yang Z, Yu HM, Wu CY, Cao GS, Xie J, Zhao XB. Preparation of nano-structured $LiFe_xMn_{1-x}PO_4$ ($x = 0$, 0.2, 0.4) by reflux method and research on the influences of Fe(II) substitution. J Mater Sci Technol. 2012;28(9):823.
[21] Du HM, Jiao LF, Wang QH, Huan QH, Guo LJ, Si YC, Wang YJ, Yuan HT. Morphology control of $CoCO_3$ crystals and their conversion to mesoporous Co_3O_4 for alkaline rechargeable batteries application. CrystEngComm. 2013;15(30):6101.
[22] Chang XY, Wang ZX, Li XH, Zhang L, Guo HJ, Peng WJ. Synthesis and performance of $LiMn_{0.7}Fe_{0.3}PO_4$ cathode material for lithium ion batteries. Mater Res Bull. 2005;40(9):1513.